ADVANCED MATERIALS
www.advmat.de

Metal-Halogen Interactions Inducing Phase Separation for Self-Healing and Tough Ionogels with Tunable Thermoelectric Performance

Wei Zhao, Yiwei Zheng, Aibin Huang, Meng Jiang, Lianjun Wang, Qihao Zhang,* and Wan Jiang**

Ionic liquid-based thermoelectric gels become a compelling candidate for thermoelectric power generation and sensing due to their giant thermopower, good thermal stability, high flexibility, and low-cost production. However, the materials reported to date suffer from canonical trade-offs between self-healing ability, stretchability, strength, and ionic conductivity. Herein, a self-healing and tough ionogel (PEO/LiTFSI/EmimCl) with tunable thermoelectric properties by tailoring metal-halogen bonding interactions, is developed. Different affinities between polymer matrix and salts are exploited to induce phase separation, resulting in simultaneous enhancement of ionic conductivity and mechanical strength. Molecular dynamics (MD) simulations and spectroscopic analyses show that Cl^- ions impair the lithium-ether oxygen coordination, leading to changes in chain conformation. The migration difference between cations and anions is thus widened and a transition from n-type to p-type thermoelectric ionogels is realized. Furthermore, the dynamic interactions of metal-ligand coordination and hydrogen bonding yield autonomously self-healing capability, large stretchability (2000%), and environment-friendly recyclability. Benefiting from these fascinating properties, the multifunctional PEO-based ionogels are applied in sensors, supercapacitors, and thermoelectric power generation modules. The strategy of tuning solvation dominance to address the trade-offs in thermoelectric ionogels and optimize their macroscopic properties offers new possibilities for the design of advanced ionogels.

1. Introduction

Ionic thermoelectric (iTE) materials based on the Soret effect have recently gained considerable interest due to their significantly larger ionic Seebeck coefficient (S_i, >1 mV K^{-1}) compared to the traditional electronic Seebeck coefficient (S_e, ≈10^2 μV K^{-1}), which endows them with great potential for applications in heat flux sensing, wearable power sources, and low-grade heat harvesting.[1,2] Among various iTE materials, ionic liquid-based ionogels offer attractive advantages such as quasi-solid state, non-volatility, good thermal stability, high flexibility, low cost, and scalable processability.[3] So far, a number of strategies have been proposed to enhance the thermoelectric performance of ionogels, such as modulation of ion-polymer interactions, ion doping, incorporation of inorganic fillers, and electrode engineering.[4–7] Yet, the growing demand for practical wearability and motion applications exacerbates the need for multifunctionality in iTE gels. There is a strong desire to develop flexible, stretchable, and tough ionogels that can withstand severe

W. Zhao, M. Jiang, L. Wang, W. Jiang
State Key Laboratory for Modification of Chemical Fibers and Polymer Materials
College of Materials Science and Engineering
Donghua University
Shanghai 201620, China
E-mail: wanglj@dhu.edu.cn; wanjiang@dhu.edu.cn

Y. Zheng
Soochow Institute for Energy and Materials Innovations
College of Energy
Key Laboratory of Advanced Carbon Materials and Wearable Energy Technologies of Jiangsu Province
Soochow University
Suzhou 215006, China

A. Huang
State Key Laboratory of High Performance Ceramics and Superfine Microstructure
Shanghai Institute of Ceramics
Chinese Academy of Sciences
Shanghai 200050, China

Q. Zhang
Light Technology Institute, Karlsruhe Institute of Technology
Engesserstrasse 13, 76131 Karlsruhe, Germany
E-mail: qihao.zhang@kit.edu

The ORCID identification number(s) for the author(s) of this article can be found under https://doi.org/10.1002/adma.202402386

DOI: 10.1002/adma.202402386

deformation while maintaining their excellent thermoelectric performance. More desirably, iTE gels should be capable of autonomously repairing mechanical damage to extend service life and reduce maintenance costs.[8]

By introducing the reversibility of dynamic interactions, some thermoelectric ionogels have been capable of self healing. For example, Jeon et al. combined a fluoro-surfactant with poly(vinylidene fluoride-co-hexafluoropropylene) (PVDF-HFP) and 1-ethyl-3-methylimidazolium trifluoromethanesulfonate to form dynamic ion-dipole interactions, which led to self healing when heated at 90 °C.[9] Huang et al. demonstrated a self-healing iTE gel by building reversible ion-dipole interactions within amorphous PVDF-HFP.[10] Recently, we reported stretchable and self-healable iTE gels by constructing reversible metal-ligand coordination bonds.[11] However, although these dynamic interactions contribute to self healing, they are always accompanied by the reduction in mechanical strength. As a result, iTE gels with low mechanical strength are susceptible for destruction when resisting various deformations. By further constructing the chemically cross-linked networks or adding rigid components into self-healing iTE gels can improve their fracture strength.[12,13] Nevertheless, the stretchability is limited due to the stiff network. In addition, self-healing iTE gels need to have high ionic conductivity to provide favorable conductive performance. The ionic conductivity can be enhanced by increasing the content of ionic liquid, but this usually results in weakened mechanical strength.[14] Overall, there is a canonical trade-off between self-healing ability, stretchability, strength, and ionic conductivity of current iTE gels. Integrating these merits simultaneously to design a self-healable, stretchable, tough, and highly conductive iTE gel remains a great challenge.

Phase separation strategies have gained much attention due to their effectiveness in simultaneously imparting excellent mechanical properties and ionic conductivity to ionogels in the field of durable skin-mimicking sensors, humidity-responsive supercapacitors and tribo/piezoelectric nanogenerators.[15–18] Taking advantage of the different interactions between the polymer chains and the surrounding solvent, phase separation occurs in the ionogel network, forming a soft solvent-rich phase and a hard polymer-rich phase.[19] The soft domain provides self-healing capability, large strain, and ionic conductivity, whereas the hard domain endows high mechanical strength and toughness.[20,21] Typically, phase-separated ionogels are prepared by methods such as copolymerization of two monomers in a common ionic liquid, polymerization of one monomer in a co-solvent system, or solvent exchange strategies.[22] Despite their effectiveness, the fact that these synthesis processes involve multiple steps or are time-consuming and labor-intensive has hindered their widespread adoption. There have been vacancies for phase separation in iTE gels.

Herein, we propose a facile one-step method to achieve phase separation for the preparation of self-healing and tough iTE gels with fast ion transport. Metal-ligand interactions within iTE gels have been tuned through the creative introduction of halogen-based ionic liquids, allowing for a change in chain conformation and thus tuning of macroscopic properties. As a demonstration, we use polyethylene oxide (PEO) polymer and lithium bis(trifluoromethanesulfonyl)imide (LiTFSI) because of their good compatibility. The formation of dynamic lithium-ether oxygen (Li-O) coordination endows the ionogel with rapid autonomous self-healing in the homogeneous amorphous binary system. Further, EmimCl is introduced, which weakens the Li-O coordination by virtue of the different affinity between ions and polymer matrix, leading to a conformational change of the PEO chains. As a result, Cl^- ions trigger the in situ phase separation, forming polymer-rich and ion-rich domains in ternary PEO/LiTFSI/EmimCl ionogel. Mechanical strength and ionic conductivity are thus simultaneously enhanced. Furthermore, the addition of EmimCl results in the shift of dominating transport ions from anions to cations, thus achieving a N-type to P-type transition of the iTE gels within the same polymer matrix. Consequently, the ternary ionogels exhibit well-optimized properties, including fracture strength and Young's modulus that are 5.5-folds and 22-folds larger than those of pristine binary ionogels, respectively, prominent stretchability (2000%), high ionic conductivity (3 mS cm^{-1}), and tunable ionic Seebeck coefficient (from −4 to 13 mV K^{-1}), while maintaining the self healing ability. In addition to these, the ternary ionogels present excellent strain sensing capability and environment-friendly recyclability. This all-in-one result provides a promising method to solve the long-standing dilemma of multiple contradictions in iTE gels and emphasizes the importance of ion interactions and polymer chain conformational change for iTE performance.

2. Results and Discussion

The initial binary iTE gels consist of PEO and LiTFSI (abbreviated as P-LT, where LiTFSI loading is 50 wt.%). These two components have excellent miscibility because of the strong coordination between lithium cations and the negatively charged ether oxygen units.[23] The $TFSI^-$ anions have a larger size and thus can effectively eliminate the crystallization and form amorphous regions to facilitate ion transport.[24] As a result, the binary iTE gels will have a homogeneous network (**Figure 1a**). However, the interactions between the PEO chains are weakened due to the excess lithium bonding and large-sized anions, which can lead to lower mechanical strength and ionic conductivity. Besides, in principle due to the strong Li-O coordination and the presence of anion clusters, P-LT ionic conductor would show a N-type iTE behavior.[11] Furthermore, we find that there are weak hydrogen bonding interactions between imidazolium cations and PEO ether oxygen segments, while there is a larger affinity between chloride anions and lithium cations. The electrostatic potential maps (Figure 1b) show that the PEO chains are tightly wrapped around Li^+ due to strong coordination, whereas $Emim^+$ has no significant effect on the arrangement of PEO chains due to the weak hydrogen bonding between ether oxygen and C-H on imidazolium ring. The lower binding energy between Li^+ and Cl^- suggests that the interaction of Li^+-Cl^- is stronger than that of PEO-Li^+ and $Emim^+$-Cl^-. This implies that the introduction of Cl^- with higher electron density can weaken Li-O coordination, and thus is expected to restore the contraction of polymer chains

W. Jiang
Institute of Functional Materials
Donghua University
Shanghai 201620, China

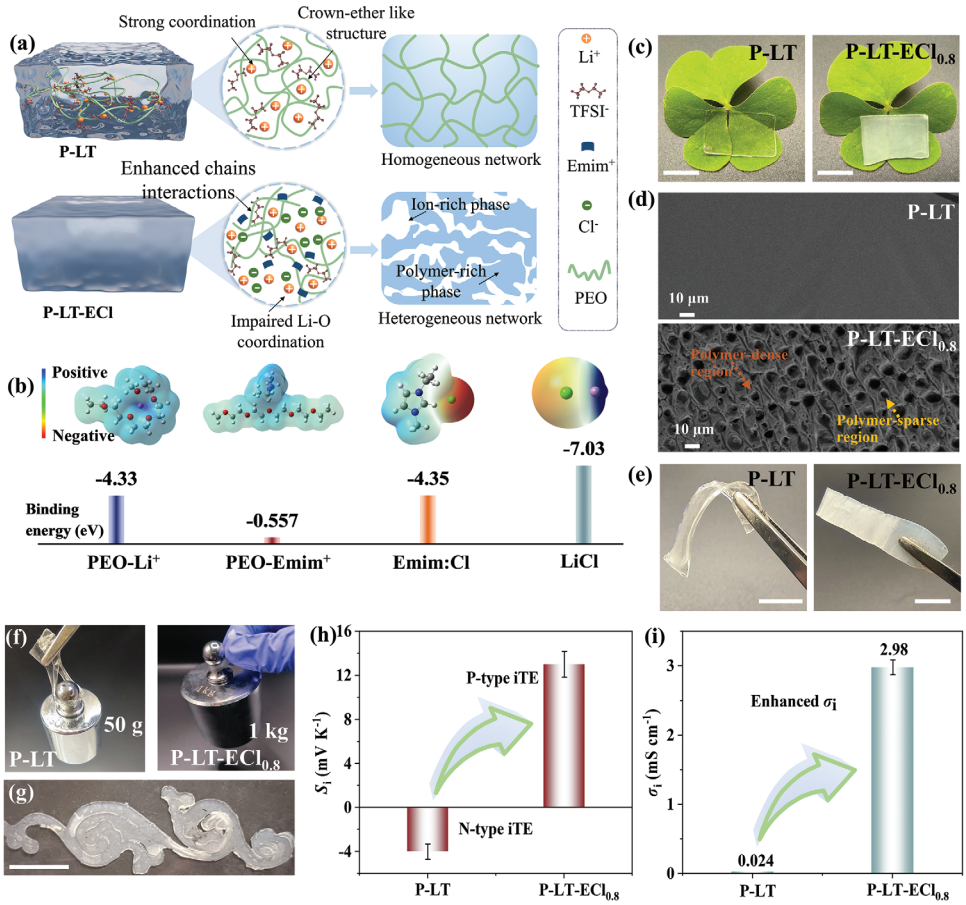

Figure 1. a) Schematic diagrams of binary PEO/LiTFSI (abbreviated as P-LT) ionic conductor with a homogeneous network and ternary PEO/LiTFSI/EmimCl (abbreviated as P-LT-ECl) ionogel with phase separation. b) Electrostatic potential maps and corresponding binding energies. c) Optical photographs of ionogels attached to leaves showing transparency contrasts. The scale bar is 1 cm. d) SEM images of ionogels with and without phase separation. e) Photographs showing the change in flexibility of the samples, from natural-sagging P-LT (left) to slightly bendable P-LT-$ECl_{0.8}$ (right). The scale bar is 1 cm. f) Photographs of P-LT and P-LT-$ECl_{0.8}$ lifting up a 50 g and 1 kg weight loads, respectively. g) A cloud-like object prepared using P-LT-$ECl_{0.8}$ ionogel demonstrating its good processibility. The scale bar is 1 cm. h) Tunable ionic Seebeck coefficient from N-type to P-type. i) Significantly enhanced ionic conductivity.

caused by strong Li-O coordination. Ultimately, a heterogeneous network will be formed due to the different interactions among the components, leading to simultaneous enhancement of thermoelectric and mechanical properties.

Experimentally, we find that the binary P-LT ionic conductors are highly transparent but turn white after the introduction of EmimCl ionic liquid (Figure 1c). The evolution of opacity is attributed to the severe light scattering from the heterogeneous network caused by phase separation.[25] Scanning electron microscopy images (Figure 1d) further display a distinct morphological change. The surface of P-LT is smooth, indicating a homogeneous network. In contrast, P-LT-$ECl_{0.8}$ ionogel exhibits a hierarchical porous structure separated by the surrounding polymer skeleton, which is associated with polymer-rich phase and ion-rich phase. Moreover, the phase images obtained by atomic force microscopy (AFM, Figure S1, Supporting Information) indicate that P-LT exhibits a uniform monophase while the phase contrast increases for P-LT-$ECl_{0.8}$, demonstrating the obvious phase separation after introducing EmimCl ionic liquid. Energy dispersive spectroscopy maps also confirm the homogeneous distribution of elements in P-LT, whereas Cl^- enrichment appears in P-LT-$ECl_{0.8}$ (Figure S2, Supporting Information). Small-angle X-ray scattering (SAXS) was further performed. The enhanced scattering intensity of P-LT-$ECl_{0.8}$ compared to that of P-LT verifies the existence of phase separation (Figure S3, Supporting Information). The absence of clear scattering peak is similar to previous reports and is ascribed to the merging of polymer-rich domains.[16] Moreover, it should be noted that the P-LT-$ECl_{0.8}$ here remains amorphous and the polymer-rich phases are prone to form by the aggregation of polymer chains under different conformations rather than crystallization, which will be discussed in the following section.

In addition, the P-LT ionic conductor is a quite soft with natural bending and sagging characteristics, whereas the P-LT-$ECl_{0.8}$ is much stiffer (Figure 1e). When lifting a weight of 50 g, the P-LT ionic conductor is stretched and P-LT-$ECl_{0.8}$ displays no obvious deformation even when lifting a weight as large as 1 kg (Figure 1f; Figure S4, Supporting Information). These behaviors suggest that phase separation leads to enhanced modulus. The effect on the mechanical strength also confers good processibility,

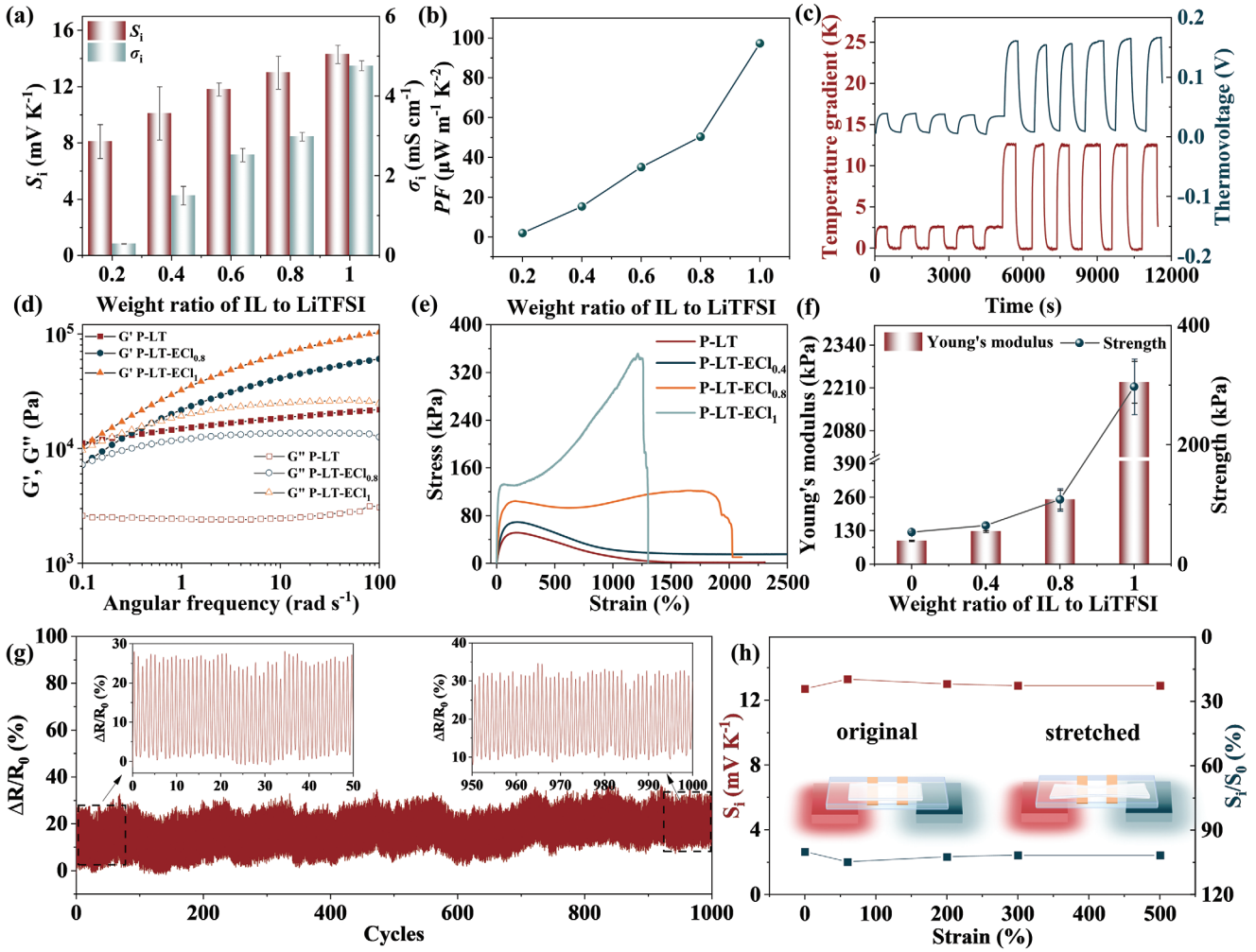

Figure 2. a) Ionic Seebeck coefficients and ionic conductivities of P-LT-ECl$_x$ ionogels with different EmimCl contents. b) Power factors. c) Continuous variations of temperature and the corresponding thermovoltage curves of P-LT-ECl$_{0.8}$. d) Dependence of storage modulus (G') and loss modulus (G") on angular frequency. e) Tensile strain-stress curves. f) Young's modulus and strength of P-LT-ECl$_x$ ionogels with different EmimCl contents. g) Relative resistance changes of P-LT-ECl$_{0.8}$ under 50% strain for 1 000 cycles. Insets are the magnified views of changes during the initial and final tests. h) Variations of ionic Seebeck coefficient for P-LT-ECl$_{0.8}$ under different strains. Insets show the schematic illustration of the measurement.

which allows for easy molding into complex three-dimensional objects (Figure 1g). More interestingly, the ionic Seebeck coefficient can be tuned from −4 mV K^{-1} to 13 mV K^{-1} (Figure 1h; Figure S5, Supporting Information) while the ionic conductivity is dramatically improved from 0.02 mS cm^{-1} to 3 mS cm^{-1} (Figure 1I; Figure S6, Supporting Information) when EmimCl is added to the binary P-LT system, resulting in a N-P transition within the same polymer matrix.

To further evaluate the effect of introducing halogen on the thermoelectric and mechanical properties, we adjusted the weight ratio of EmimCl to LiTFSI. As shown in **Figure 2a**, both ionic Seebeck coefficient and conductivity increase with the increasing EmimCl content. When the weight ratio of EmimCl to LiTFSI is 100%, the Seebeck coefficient and conductivity rise to 14 mV K^{-1} and 4.8 mS cm^{-1}, respectively. Correspondingly, the ionic power factors increase dramatically from 1.9 to 97.3 μW m^{-1} K^{-2} (Figure 2b). These thermoelectric properties were measured at relative humidity (RH) of 50%.

The influence of humidity on the ionic Seebeck coefficient and ionic conductivity of P-LT-ECl$_{0.8}$ was further investigated. As shown in Figure S7 (Supporting Information), the S_i increases from 11.8 to 25.1 mV K^{-1} when RH increases from 30% to 90%. The σ_i displays a prominent enhancement with the increasing RH and the maximum value achieves 8.58 mS cm^{-1} at 90% RH (Figure S8, Supporting Information). The thermal conductivities (λ_i) of P-LT-ECl$_x$ ionogels were measured by using the transient hot-wire method. As shown in Figure S9 (Supporting Information), the thermal conductivity is insensitive to the EmimCl contents and all samples possess low λ_i ≈0.35 W m^{-1} K^{-1}. The inherent low λ_i enables the ionogels to maintain a temperature gradient and realize a stable thermal voltage output. The ternary P-LT-ECl ionogel shows a fast and repeatable temperature response during multiple heat-on and heat-off cycles (Figure 2c).

Contrary to previous work based on dynamic physical crosslinking to optimize iTE properties at the expense of mechanical strength, the P-LT-ECl ternary ionogels in this work achieve

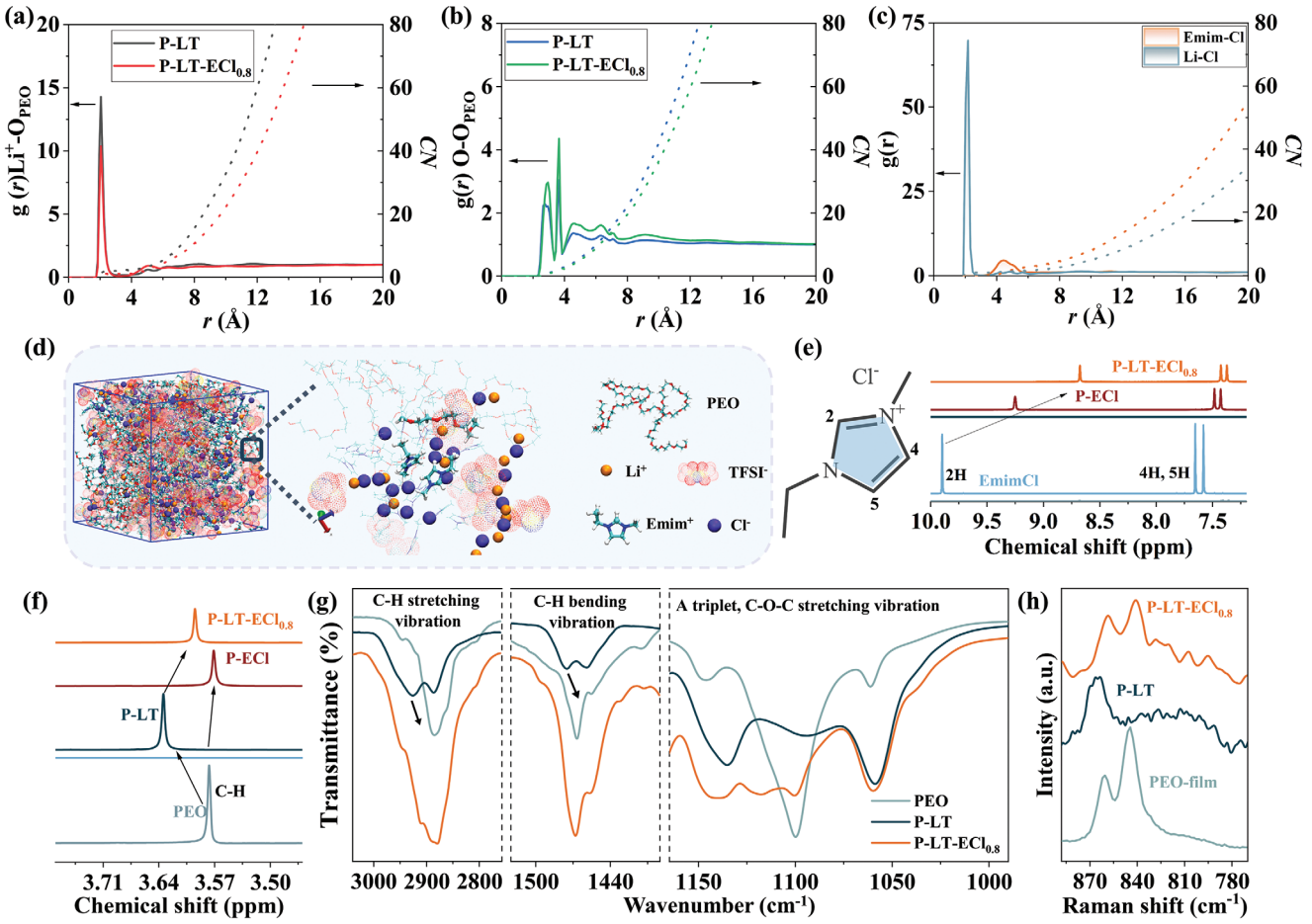

Figure 3. a) RDF and CN of Li^+-O_{PEO} binding in P-LT and P-LT-$ECl_{0.8}$. b) RDF and CN of O_{PEO}-O_{PEO} binding. c) RDF and CN of Li^+-Cl^- pair and $Emim^+$-Cl^- pair. d) MD snapshot of P-LT-$ECl_{0.8}$, displaying the coordination environment. e). H-NMR spectra revealing the chemical shift of H on imidazolium cations. f) H-NMR spectra revealing the chemical shift of H on PEO chains. g) FTIR spectra showing the stretching and bending vibration band of C-H and the stretching vibration band of C-O-C. h) Raman spectra in the C-H rocking region.

simultaneous enhancement of thermoelectric and mechanical properties. Rheological measurements were conducted to analyze the viscoelastic characteristics of ionogels with different EmimCl contents. As shown in Figure 2d, the storage modulus *G'* increases with the increasing EmimCl loading. For the binary P-LT gel, *G'* is always higher than loss modulus (*G″*) in the angular frequency range of 0.1–100 $rads^{-1}$, indicating its elastic characteristics. By contrast, for the ternary P-LT-$ECl_{0.8}$ and P-LT-ECl_1, *G'* and *G″* intersect at low frequencies and both increase with frequency, which is an indicator of enhanced viscoelasticity.[26] The mechanical properties were further investigated by tensile measurements. Figure 2e shows the strain-stress curves of P-LT-ECl_x ionogels. A notable strengthening effect depending on the EmimCl loading can be observed, where higher EmimCl loading results in higher tensile strength. Besides, the Young's modulus, tensile strength and toughness are all significantly enhanced (Figure 2f; Figure S10, Supporting Information). This is attributed to halogen-induced phase separation that recovers the inter/intra-polymer chain interactions and endows the P-LT-ECl ionogel with higher toughness by viscoelastic energy dissipation.[27] Despite the elongation at break decreasing with increasing Young's modulus, the P-LT-$ECl_{0.8}$ sample still exhibits super-stretchability of 2000%. In addition, P-LT-$ECl_{0.8}$ demonstrates favorable reliability and fatigue resistance during the successive stretching-releasing cycling test (Figure 2g). More critically, the ionic Seebeck coefficient shows great stability under different strains, even as large as 500% (Figure 2h). These results validate the effectiveness of the phase-separated structure to provide decent ionic conductivity through the solvent-rich regions and to enhance the mechanical properties through the polymer-rich regions.

To gain in-depth understanding of the interactions within ionogels and to analyze their effect on the macroscopic properties, we performed molecular dynamics (MD) simulations. The radial distribution functions (RDFs) and coordination numbers (CNs) elucidate the arrangement of ether oxygen from PEO chains and anions distributed around Li^+ in P-LT and P-LT-$ECl_{0.8}$. The sharp peak at a distance of 2.05 Å in the Li^+-O_{PEO} RDF suggests that the ether oxygens in PEO chains and the $TFSI^-$ occupy the first coordination shell of Li^+ (**Figure 3a**; Figure S11, Supporting Information). The ether oxygens are helically coordinated with Li^+ (Figure S12, Supporting Information). PEO chains tightly wrap Li^+ in a preferably crown-ether-like conformation, resulting in a contraction of the conformational phase space.[28,29]

In contrast, the solvated sheath of Li^+ is significantly changed after the addition of EmimCl. It can be observed that the coordination oxygen concentration in P-LT-$ECl_{0.8}$ is reduced compared to that in P-LT. The lower CN of O (≈2.5) in the first solvation shell of P-LT-$ECl_{0.8}$ compared to that of P-LT (≈5.4) indicates that Li^+-O_{PEO} coordination is weakened.[30] In addition, the RDF between ether oxygen atoms in PEO chains shows a higher amplitude for P-LT-$ECl_{0.8}$ than P-LT (Figure 3b), which suggests greater structure heterogeneity.[31] Due to the release of coordinated ether oxygen, the peak for O_{PEO}-O_{PEO} in P-LT-$ECl_{0.8}$ locates at a larger distance with a smaller CN.[29] Moreover, there is an extremely sharp peak at 2.17 Å for the Li^+-Cl^- pair, whereas $Emim^+$-Cl^- has a small peak (Figure 3c), reflecting the fact that the introduced Cl^- anions coordinate more strongly with Li^+ than with $Emim^+$. As a result, Li^+-O_{PEO} coordination can be weakened because Li^+ prefer to coordinate with Cl^- in P-LT-$ECl_{0.8}$.

The local structure change can be visualized in the snapshots of Figure 3d and Figure S12 (Supporting Information). The decoupling of Li^+ from the crown-ether like PEO chains not only changes the conformations in the presence of Cl^-, but also partially contributes to the complete release Li^+ from the PEO host to form the Li^+-Cl^- ions pair. The strong binding of Cl^- by Li^+ can effectively drag the transport of Cl^- anions, and thus enhance the migration difference between $Emim^+$ and Cl^-.[5] In addition, the less coordinated $TFSI^-$ clusters and more loosely coordinated $Emim^+$ by Cl^- can reduce the anion transfer entropy while enlarging the $Emim^+$ transfer entropy, which contributes to the transition from N-type to P-type thermoelectric ionogels.[6]

The interactions within ionogels are further verified via nuclear magnetic resonance (NMR), Fourier transform infrared (FTIR), and Raman spectroscopy. First, it can be seen from H-NMR that there is an upward shift for the C^2-H on $Emim^+$ in P-LT-$ECl_{0.8}$ compared to that of P-ECl (Figure 3e). This indicates a weaker hydrogen bonding between C^2-H and Cl^- due to the stronger Li^+-Cl^- interaction. In addition, in P-LT, the coordination of Li^+ lowers the electron density around H on the PEO chains (Figure 3f), which leads to higher H chemical shift originating from the deshielding effect.[32] However, in P-LT-$ECl_{0.8}$, the H belonging to PEO undergoes upfield shifts due to the weakening of Li^+ coordination and the upward shift increases with the increasing EmimCl contents (Figure S13, Supporting Information). FTIR spectra further confirm the change in coordination (Figure 3g; Figure S14a, Supporting Information). The C-H stretching and bending vibrations of PEO chains are observed at 2760 to 3060 cm^{-1} and 1400 to 1520 cm^{-1}, respectively. Notably, the splitting peaks in P-LT resulting from Li^+ coordination are remerged into a single peak after adding EmimCl. The C-O-C stretching vibration near 1100 cm^{-1} is associated with the crystallization of PEO, which is sensitive to alkali metal coordination.[33] The coordination of Li^+ leads to a significant decrease in the intensity of the band at 1104 cm^{-1} and a redshift from 1148 to 1135 cm^{-1} relative to the PEO matrix. Nevertheless, when EmimCl is introduced, the peak at 1135 cm^{-1} shifts to a higher wavenumber and the peak at 1104 cm^{-1}, associated with uncoordinated ether oxygen, reappears. This implies that the Li^+-ether oxygen coordination has been impaired. At the same time, the intensity of Cl^- interaction band at 3049 cm^{-1} in pure EmimCl decreases and its peak shifts to 3118 cm^{-1}. This indicates that the C^2H-Cl interactions are weakened due to the formation of more electronegative Li^+-Cl^- bond (Figure S14b, Supporting Information),[34,35] which enhances the cation contribution to ionic thermopower.

The ion complexation results in conformational changes of PEO as revealed by Raman spectra (Figure 3h; Figure S15a, Supporting Information). Upon Li^+ complexation with ether oxygen, the peak at 845 cm^{-1} of PEO disappears and a new band appears ≈866 cm^{-1}. But the peaks with similar shape to that of PEO is recovered in P-LT-$ECl_{0.8}$. The peak frequency is decreased, indicating an increase in the O-C-C-O torsional angle,[36] which is in accordance with the MD simulations. Interestingly, this phenomenon can be observed in other PEO-based ionogels (Figure S15b,c, Supporting Information). For n-type ionogels such as the previously reported PEO-LiTFSI-$EmimBF_4$[11] and PEO-LiTFSI-$EmimPF_6$ in this work, the peak ≈845 cm^{-1} disappears from the Raman spectrum and the band frequency increases to 871 cm^{-1}, manifesting that PEO chains in n-type ionogels have a crown-ether like conformation. In regard to p-type ionogels such as the previously reported PEO-EmimOAC,[4] PEO-P123-EmimOAC[4] and P-LT-$ECl_{0.8}$ in this work, there are peak shapes and frequencies similar to those of pure PEO, implying that they have the conformation with a large torsional angle. Therefore, the coordination-induced conformational change has a dramatic effect on ion transport, where the former with a crown-ether like conformation facilitates anion transport while the later contributes to cation transport. Furthermore, the modulation of EmimCl enriches the PEO conformation, which can generate new nanostructures and lead to phase separation related to ionic conductivity and mechanical properties.[37] These results support the hypothesis that the introduction of halogens can tailor the lithium solvation structure and PEO chain conformation, ultimately promoting chain interactions and greater cation transfer contributions.

The rational design of P-LT-ECl ionogel with fascinating interactions endows it with multifunctionality in addition to high thermoelectric properties, such as mechanical robustness, fast self-healing capability and recyclability. For example, a strip of P-LT-$ECl_{0.8}$ ionogel can be attached onto a finger to monitor its movement. As shown in **Figure** 4a, the change in resistance increases when deepening the finger flexion, while it remains nearly constant when the finger is held a certain angle. There is a fast and repeatable response during multiple bending and straightening motions (Figure 4b). In addition, the abundant Li^+-O_{PEO} coordination in the amorphous network facilitates fast and reversible reconstruction (Figure 4c), which enables the breakage to heal spontaneously.[38] The step-strain rheological analysis at different strains (5% and 200%) was also performed to verify the self-healing property of P-LT-$ECl_{0.8}$ (Figure S16, Supporting Information). The storage modulus recovers rapidly after large strain-induced damage. The rate and extent of recovery remain almost unchanged during three cycles of fracture and self-healing, indicating favorable self-healing property. As demonstrated in Figure 4d, scratches of tens of micrometers in P-LT-$ECl_{0.8}$ disappear after healing at room temperature without applying any external stimuli. It should be mentioned that the humidity can also boost the self healing process. As shown in Figure S17 (Supporting Information), the scratch in the P-LT-$ECl_{0.8}$ ionogel at low RH of 30% disappears within 3 h. When RH is increased, the cracks diminish after 30 min at RH of 60% and 90%.

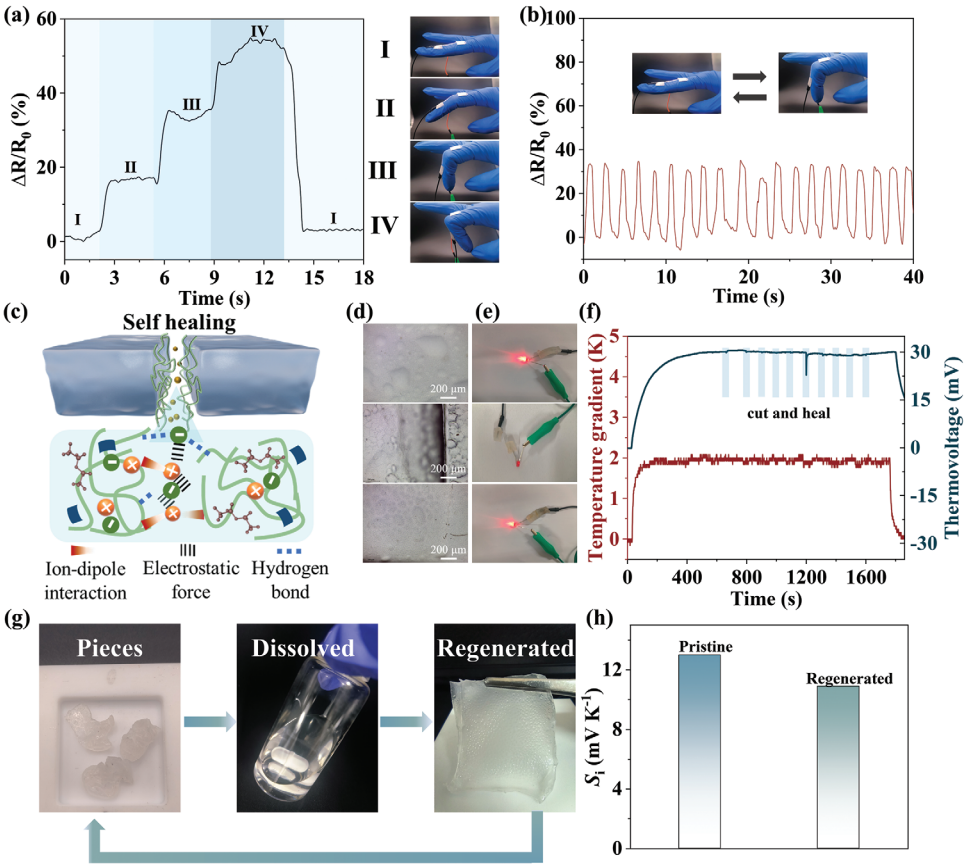

Figure 4. a) Attaching ionogel on a finger as a sensor to monitor the resistance change at different bending angles. b) Change in resistance during repeated bending movements. c) Schematic illustration of the self-healing mechanism. d) Optical microscopy images of the broken ionogel before and after self healing. e) Demonstration of rapid autonomous self healing by connecting the ionogel to a light-emitting diode (LED). f) Change of thermovoltage with multiple cut-healing cycles. g) Flow diagram of recyclability and reconstitution of P-LT-ECl$_{0.8}$ ionogel. h) Ionic Seebeck coefficients of pristine and regenerated ionogels.

In addition, a sample that is cut into two pieces and colored red and blue can effectively heal and then withstand a great deal of stretching (Figure S18, Supporting Information). Further, the P-LT-ECl$_{0.8}$ ionogel can be used as a conductor connected in a circuit to light up an LED bulb due to its commendable ionic conductivity (Figure 4e). When the ionogel is cut in half, the LED is extinguished; it can be re-lighted immediately after connecting the two pieces, demonstrating the rapid recovery of the circuit. Remarkably, the ionogel can withstand multiple cycles of cutting and self healing (Figure 4f). The generated thermal voltage recovers instantly and a stable and reliable output voltage is guaranteed. Moreover, the pristine ionogel shows an average S_i of 13.3 mV K^{-1}, which still remains at 13.1 mV K^{-1} after the self healing process (Figure S19, Supporting Information).

It is worth noting that the introduction of Cl^- impairs the Li^+-O_{PEO} coordination and leads to changes in the aggregation of the polymer chains. Excessive amounts of EmimCl even result in the reappearance of crystallization in the ionogels (Figure S20, Supporting Information). In this regard, we also analyze the effect of EmimCl loading content on the self healing property. It can be observed under optical microscopy that the scratches disappear in the ionogel with EmimCl loading of 0–80%, but the scratches still exist in P-LT-ECl$_1$ (Figure S21, Supporting Information). This indicates that the addition of excess EmimCl disables the self-healing ability, which is consistent with the severely weakened Li^+-O_{PEO} coordination and sluggish dynamics.

Benefiting from dynamic physical interactions in the network rather than chemical cross-linking, the P-LT-ECl$_{0.8}$ ionogel presents green recyclability.[39] As is demonstrated in Figure 4g, the broken ionogel fragments are placed into ethanol and can be dissolved to form a clear solution. Then, the ionogel can be regenerated by evaporation of the solvent. The regenerated ionogel has similar ionic Seebeck coefficient and ionic conductivity to the pristine ionogel (Figure 4h; Figure S22, Supporting Information). Besides, the strain-stress curves in Figure S23 (Supporting Information) indicate that the regenerated ionogels still have large stretchability and tensile strength close to the pristine ionogels. These results confirm the satisfactory recycling performance. This feature is essential for achieving sustainable use of energy and alleviating the E-waste crisis.

Different from the traditional thermoelectric devices that rely on electrons and holes as carriers, thermoelectric ionogels based on the Soret effect cannot be used directly as generators because ionic carriers cannot be transported through the electrode interface into external circuits. Alternatively, we can

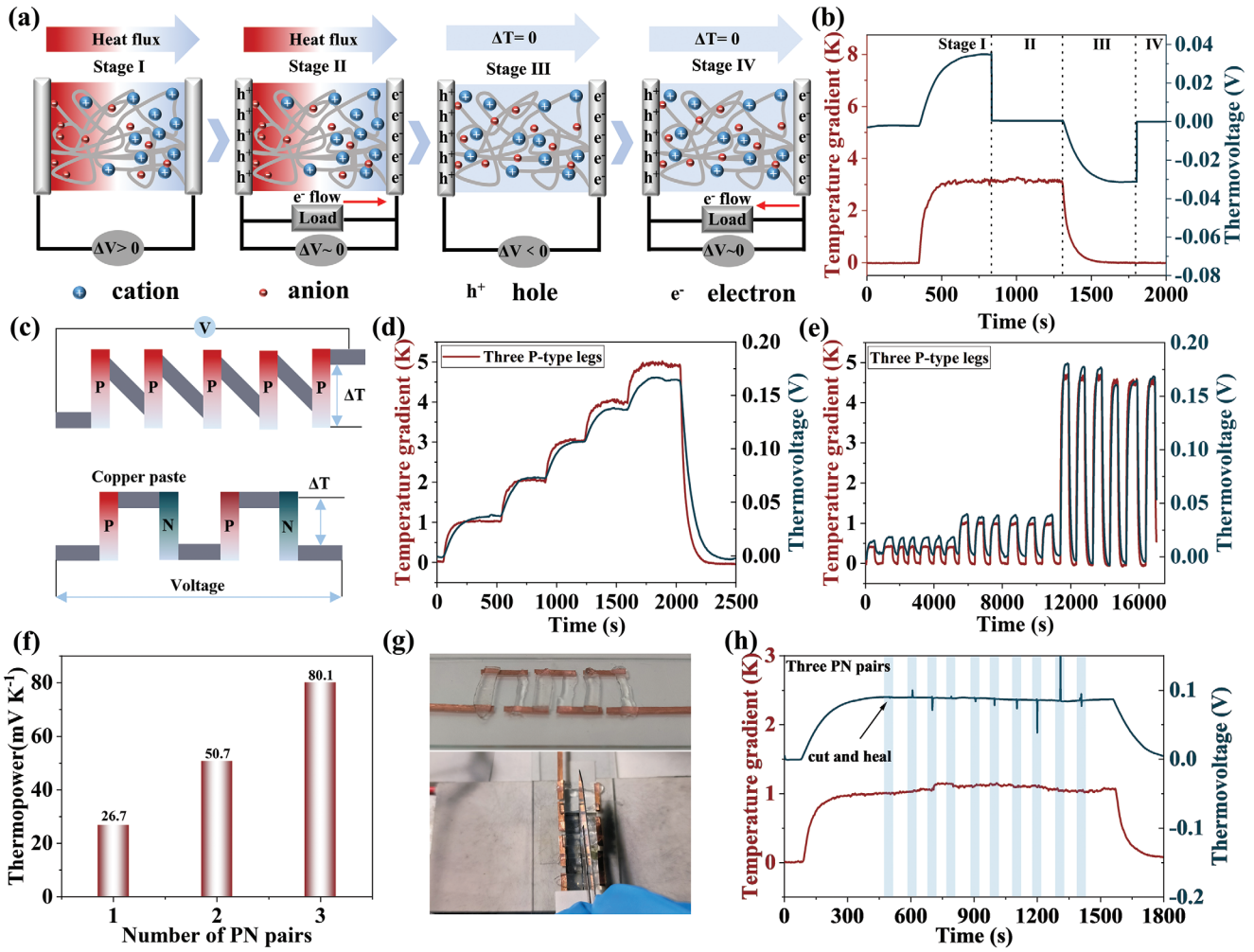

Figure 5. a) Schematic illustration of the operation of an iTE capacitor. b) Thermovoltage profiles under given temperature gradients of an iTE capacitor assembled with P-LT-ECl$_{0.8}$ and Cu electrodes. c) Schematic illustration of iTE modules composed of only P-type legs or P-N pairs. d) Temperature gradient and corresponding thermovoltage of an iTE module consisting of three P-type P-LT-ECl$_{0.8}$ legs. e) Continuous variation of temperature and corresponding thermovoltage, showing excellent thermal response. f) Increasing thermopower with the increasing number of P-N pairs. g) Photograph of cutting P-N legs by a scissor. h) Multiple cutting and self-healing cycling tests on P-N legs.

achieve heat-to-electricity conversion by assembling iTE capacitors (**Figure** 5a,b).[40,41] In principle, there are four stages within a thermal cycle. For example, when a temperature gradient of 3 K is applied to the device at stage I, cations (P-type) dominantly diffuse from the hot side to the cold side and reach equilibrium with the cations and anions being accumulated on the hot and cold electrodes, respectively. As a result, an open-circuit voltage of 35 mV is generated. Then, an external resistance load of 1 kΩ is connected at stage II, which causes electrons to migrate from the external circuit to the electrodes and thus balance the thermovoltage by ion accumulation. In this case, the voltage quickly decays to zero. Once the temperature gradient and external resistance load are removed at stage III, the ions accumulated on the electrodes recover to their original distribution while the electrons and holes are retained on the electrodes, resulting in a reverse voltage. Finally, when the external load is reconnected at stage IV, electrons flow out through the external circuit and the voltage drops to zero.

In order to further increase the output voltage signal or to enhance the sensitivity to heat, we can connect multiple thermoelectric legs in electrical series. Figure 5c displays the structure of thermoelectric modules consisting of only P-type legs and P-N pairs. As a showcase, when integrating multiple P-type P-LT-ECl$_{0.8}$ legs, the thermopower increases from 11.6 mV K^{-1} for one leg to 59.8 mV K^{-1} for five legs (Figure S24, Supporting Information). The module shows a real-time response to changes of temperature gradient and stable thermovoltage output (Figure 5d). During repeated heat-cooling cycles at different temperature gradients, the thermovoltage is reproducible (Figure 5e), demonstrating good reliability. However, the module consisting of only P-type legs inevitably suffers from heat loss caused by the electrodes. To overcome this problem, P-N pairs are required to construct complete modules with minimal heat losses. Herein, PEO-LiTFSI-EmimBF$_4$ ionogel is used as the n-type leg,[11] which has an ionic conductivity (1.86 mS cm^{-1}) and ionic Seebeck coefficient (−15 mV K^{-1}) matching that of P-type P-LT-ECl$_{0.8}$. As a

result, the thermopower is prominently improved through the integration, reaching 80.1 mV K^{-1} with only three P-N pairs. More critically, both P-type and N-type legs here possess excellent self-healing capabilities. The output thermovoltage remains stable due to the fast self healing during repeated cutting (Figure 5g,h), which will greatly extend the device lifetime and reduce maintenance costs.

3. Conclusion

In summary, we demonstrate a solvation design strategy for the synthesis of multifunctional thermoelectric ionogels. By introducing EmimCl to the binary PEO-LiTFSI, the strong Li-ether oxygen coordination is weakened, and a chain conformational change is achieved from crown-ether like to that with increasing O-C-C-O torsional angle. Spectroscopic analysis shows that the former conformation facilitates anion migration, while the latter benefits cation migration. The different affinities among LiTFSI, EmimCl, and PEO lead to phase separation and the formation of polymer-rich and ion-rich regions, which enables the simultaneous enhancement of the ionic conductivity and mechanical strength. Furthermore, the retained amorphous structure as well as dynamic Li-O coordination and hydrogen bonding contribute to large stretchability, excellent self healing, and green recyclability. Taken together, this work provides a versatile approach to solve the long-standing dilemma of multiple paradoxes in thermoelectric ionogels and will enrich the development of novel thermoelectric ionogels with superior integrated functionality.

4. Experimental Section

A detailed experimental section can be found in Supporting Information.

Supporting Information

Supporting Information is available from the Wiley Online Library or from the author.

Acknowledgements

This work was supported by the National Natural Science Foundation of China (51871053 and U23A20685), the Innovation Program of Shanghai Municipal Education Commission (202101070003E00110), Shanghai Committee of Science and Technology (20JC1415200).

Open access funding enabled and organized by Projekt DEAL.

Conflict of Interest

The authors declare no conflict of interest.

Data Availability Statement

The data that support the findings of this study are available from the corresponding author upon reasonable request.

Keywords

ionic electrical conductivity, mechanical strength, phase separation, self-healing thermoelectric ionogels

Received: February 15, 2024
Revised: April 14, 2024
Published online:

[1] B. Kim, J. U. Hwang, E. Kim, *Energy Environ. Sci.* **2020**, *13*, 859.
[2] C. G. Han, X. Qian, Q. Li, B. Deng, Y. Zhu, Z. Han, W. Zhang, W. Wang, S. P. Feng, G. Chen, *Science* **2020**, *368*, 1091.
[3] Y. H. Pai, J. Tang, Y. Zhao, Z. Liang, *Adv. Energy Mater.* **2022**, *13*, 2202507.
[4] W. Zhao, T. Sun, Y. Zheng, Q. Zhang, A. Huang, L. Wang, W. Jiang, *Adv. Sci.* **2022**, *9*, 2201075.
[5] Z. Liu, H. Cheng, Q. Le, R. Chen, J. Li, J. Ouyang, *Adv. Energy Mater.* **2022**, *12*, 2200858.
[6] S. Liu, Y. Yang, H. Huang, J. Zheng, G. Liu, T. H. To, B. Huang, *Sci. Adv.* **2022**, *8*, eabj3019.
[7] S. Mardi, D. Zhao, K. Tybrandt, A. Reale, X. Crispin, *Adv. Mater. Interfaces* **2022**, *9*, 2201058.
[8] D. H. Kim, Z. A. Akbar, Y. T. Malik, J. W. Jeon, S. Y. Jang, *Nat. Commun.* **2023**, *14*, 3246.
[9] Z. A. Akbar, Y. T. Malik, D. H. Kim, S. Cho, S. Y. Jang, J. W. Jeon, *Small* **2022**, *18*, 2106937.
[10] S. Liu, Y. Yang, S. Chen, J. Zheng, D. G. Lee, D. Li, J. Yang, B. Huang, *Nano Energy* **2022**, *100*, 107542.
[11] W. Zhao, Y. Zheng, M. Jiang, T. Sun, A. Huang, L. Wang, W. Jiang, Q. Zhang, *Sci. Adv.* **2023**, *9*, eadk2098.
[12] J. Xu, H. Wang, X. Du, X. Cheng, Z. Du, H. Wang, *ACS Appl. Mater. Interfaces* **2021**, *13*, 20427.
[13] Z. A. Akbar, J. W. Jeon, S. Y. Jang, *Energy Environ. Sci.* **2020**, *13*, 2915.
[14] Z. Cao, H. Liu, L. Jiang, *Mater. Horiz.* **2020**, *7*, 912.
[15] T. Li, Y. Wang, S. Li, X. Liu, J. Sun, *Adv. Mater.* **2020**, *32*, 2002706.
[16] M. Wang, P. Zhang, M. Shamsi, J. L. Thelen, W. Qian, V. K. Truong, J. Ma, J. Hu, M. D. Dickey, *Nat. Mater.* **2022**, *21*, 359.
[17] L. Yao, X. Ming, C. Lin, X. Duan, H. Zhu, S. Zhu, Q. Zhang, *Aggregate* **2022**, *4*, e249.
[18] T. Huang, Y. Zhang, P. He, G. Wang, X. Xia, G. Ding, T. H. Tao, *Adv. Mater.* **2020**, *32*, 1907336.
[19] Z. Wang, M. Heck, W. Yang, M. Wilhelm, P. A. Levkin, *Adv. Funct. Mater.* **2023**, 2300947.
[20] J. Tie, Z. Mao, L. Zhang, Y. Zhong, H. Xu, *Adv. Funct. Mater.* **2023**, *33*, 2307367.
[21] J. Zhang, J. Yin, N. Li, H. Liu, Z. Wu, Y. Liu, T. Jiao, Z. Qin, *Macromolecules* **2022**, *55*, 10950.
[22] K. Sato, T. Nakajima, T. Hisamatsu, T. Nonoyama, T. Kurokawa, J. P. Gong, *Adv. Mater.* **2015**, *27*, 6990.
[23] J. Chattoraj, D. Diddens, A. Heuer, *J. Chem. Phys.* **2014**, *140*, 024906.
[24] S. J. Wen, T. J. Richardson, D. I. Ghantous, K. A. Striebel, P. N. Ross, E. J. Cairns, *J. Electroanal. Chem.* **1996**, *408*, 113.
[25] M. Li, H. Lu, M. Pi, H. Zhou, Y. Wang, B. Yan, W. Cui, R. Ran, *Adv. Sci.* **2023**, *10*, 2304780.
[26] F. Zhu, S. Feng, Z. Wang, Z. Zuo, S. Zhu, W. Yu, Y. N. Ye, M. An, J. Qian, Z. L. Wu, Q. Zheng, *Macromolecules* **2023**, *56*, 5881.
[27] T. Nonoyama, Y. W. Lee, K. Ota, K. Fujioka, W. Hong, J. P. Gong, *Adv. Mater.* **2020**, *32*, 1905878.
[28] D. Diddens, A. Heuer, *J. Phys. Chem. B* **2014**, *118*, 1113.
[29] S. Xie, B. Zhang, Y. Mao, L. He, K. Hong, F. S. Bates, T. P. Lodge, *Macromolecules* **2020**, *53*, 7141.
[30] H. Y. Zhou, Y. Ou, S. S. Yan, J. Xie, P. Zhou, L. Wan, Z. A. Xu, F. X. Liu, W. L. Zhang, Y. C. Xia, K. Liu, *Angew. Chem., Int. Ed.* **2023**, *62*, e202306948.

[31] C. Chi, M. An, X. Qi, Y. Li, R. Zhang, G. Liu, C. Lin, H. Huang, H. Dang, B. Demir, Y. Wang, W. Ma, B. Huang, X. Zhang, *Nat. Commun.* **2022**, *13*, 221.
[32] S. K. Pedersen, K. Eriksen, N. N. Karaush-Karmazin, B. Minaev, H. Ågren, G. V. Baryshnikov, M. Pittelkow, *Angew. Chem., Int. Ed.* **2020**, *59*, 5144.
[33] F. Fu, Y. Zheng, N. Jiang, Y. Liu, C. Sun, A. Zhang, H. Teng, L. Sun, H. Xie, *Chem. Eng. J.* **2022**, *450*, 137776.
[34] A. Lahiri, R. Das, *Mater. Chem. Phys.* **2012**, *132*, 34.
[35] K. M. Dieter, C. J. Dymek, N. E. Heimer, J. W. Rovang, J. S. Wilkes, *J. Am. Chem. Soc.* **1988**, *110*, 2722.
[36] R. Frech, W. Huang, *Macromolecules* **1995**, *28*, 1246.
[37] C. E. Sing, J. W. Zwanikken, M. O. de la Cruz, *Nat. Mater.* **2014**, *13*, 694.
[38] T. Munaoka, X. Yan, J. Lopez, J. W. F. To, J. Park, J. B. H. Tok, Y. Cui, Z. Bao, *Adv. Energy Mater.* **2018**, *8*, 1703138.
[39] W. Li, L. Li, Z. Liu, S. Zheng, Q. Li, F. Yan, *Adv. Mater.* **2023**, *35*, 2301383.
[40] D. Zhao, H. Wang, Z. U. Khan, J. Chen, R. Gabrielsson, M. P. Jonsson, M. Berggren, X. Crispin, *Energy Environ. Sci.* **2016**, *9*, 1450.
[41] H. Cheng, X. He, Z. Fan, J. Ouyang, *Adv. Energy Mater.* **2019**, *9*, 1901085.